



Nanoscale

**Surface-Assisted Self-Assembly of 2D, DNA Binary Crystals**

Journal:	<i>Nanoscale</i>
Manuscript ID	NR-COM-03-2023-001187.R1
Article Type:	Communication
Date Submitted by the Author:	01-May-2023
Complete List of Authors:	Liu, Longfei; Yale University, Cell biology; Mao, Dake; Purdue University, Department of Chemistry Li, Zhe; Purdue University Zheng, Mengxi; Purdue University He, Kai; Hunan University of Medicine, Mao, Chengde; University of Purdue, Department of Chemistry

SCHOLARONE™  
Manuscripts

## Surface-Assisted Self-Assembly of 2D, DNA Binary Crystals

Longfei Liu<sup>1</sup>, Dake Mao<sup>1</sup>, Zhe Li<sup>1</sup>, Mengxi Zheng<sup>1</sup>, Kai He<sup>1,2</sup>, and Chengde Mao<sup>1\*</sup>

<sup>1</sup>Department of Chemistry, Purdue University, West Lafayette, IN 47907, USA

<sup>2</sup>Hunan University of Medicine, School of Pharmaceutical Science, Huaihua 418000, China

Email: mao@purdue.edu

**Abstract.** Surface-assisted, tile-based DNA self-assembly is a powerful way to construct large, two-dimensional (2D) nanoarrays. To further increase the structural complexity, one idea is to incorporate different types of tiles into one assembly system. However, different tiles have different adsorption strengths to the solid surface. The differential adsorptions make it difficult to control effective molar ratio between different DNA tile concentrations on solid surface, leading to assembly failures. Herein, we propose a solution to this problem by engineering the tiles with comparable molecular weights while maintaining their architectures. As a demonstration, we have applied this strategy to successfully assemble binary DNA 2D arrays out of very different tiles. We expect that this strategy would facilitate assembly of other complicated nanostructures as well.

Tile-based DNA self-assembly is an excellent platform to fabricate 2D nanostructures.<sup>1-10</sup> In recently years, surface-assisted, tile-based DNA self-assembly has emerged as an efficient way to assemble large-area nanoarrays.<sup>11-15</sup> However, most resulting structures are simple because often only one type (in term of overall architecture) of DNA tile is involved. To increase the capability of assembly of complicated structures, it requires multiple tiles with different architecture and different molecular weights at specific molar ratios. In surface-assisted DNA self-assembly, DNA tiles first loosely adsorb onto solid surface and then move and re-arrange themselves into regular 2D arrays. Our previous study has demonstrated that DNA tiles of smaller sizes required higher cation concentrations, i.e. stronger DNA-surface interaction, to form arrays on the surface.<sup>13</sup> When two tiles are dramatically different in architecture and molecular size, they will have very different adsorption capabilities, the effective concentration ratio between the DNA tiles adsorbed on solid surface will be very different to that in bulk solution. A problem will rise as: how to control the tile concentration ratio on solid surface by adjusting the tile concentration ratio in bulk solution? Herein, we have addressed this issue by designing tiles to have similar adsorption strength.

Our strategy is demonstrated by self-assembly of a plane of rhombille tiling (Figure 1), which is a tessellation of identical 60° rhombi (Figure 1a). The inner angles of the rhombus are alternating 60° and 120°. Three rhombi meet at the 120° vortexes and six rhombi meet at the 60° vortex. In the lattice, there are two sets of vortexes (Figure 1b). One has a connectivity of three and the other has a connectivity of six. The ratio between these two types of vortexes is 2:1. Such a lattice cannot be assembled from a single set of small DNA tiles, but can be assembled from a set of two different tiles: 3- and 6-pointed star (3PS and 6PS) motifs, representing the two different sets of vortexes, respectively (Figure 1c).

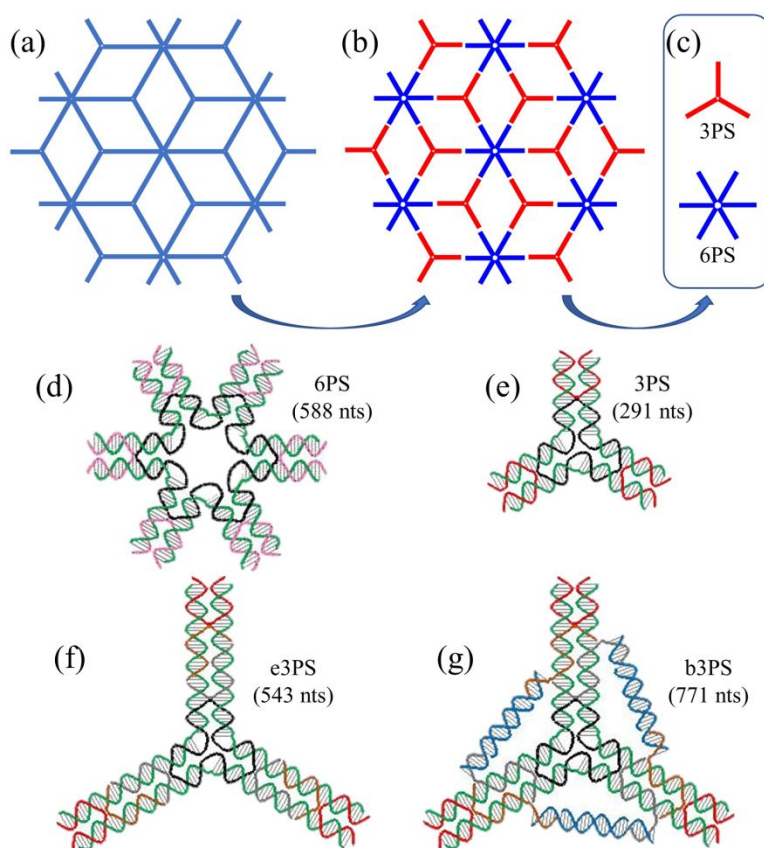


**Figure 1.** Self-assembly of a binary rhombille tiling lattice. (a) The rhombille tiling. (b) Dissection of the rhombille tiling into two sets of tiles with connectivity of three (red) and six (blue), respectively. (c) Simple schemes of 3- and 6-point stars (3PS and 6PS). Note that 3PS and 6PS have hetero- but not homo-complementary, two-nucleotide (nt)-long sticky ends. Structural schemes of DNA tiles: (d) small 6PS (6PS), (e) small 3PS (3PS), (f) elongated 3PS (e3PS), and (g) bridged 3PS (b3PS). All branches in a motif are related with each other by a rotational symmetry. The branches are two helical turns long for 3PS and 6PS, and four helical turns long for e3PS and b3PS. The size of each tile (in term of nucleotides, nts) is indicated.

Figure 1 illustrates the assembly of a binary rhombille tiling lattice from symmetric, DNA 3PS and 6PS tiles. Each tile contains multiple branches, which are related with each other by a rotational symmetry (Figure. 1d-g). Each branch consists of two parallel DNA duplexes, which are interconnected by strand crossovers. At the peripheral ends, each DNA duplex has a two-nucleotide (nt)-long sticky ends. To ensure that each 3PS motif interacts with three 6PS motifs and each 6PS motif interacts with six 3PS motifs, the sticky ends of 3PS and 6PS tiles are complementary between unlike tiles, but not complementary between like tiles. In this study, 6PS only has one design (6PS), but 3PS tile has three different designs: small (3PS), elongated (e3PS), and bridged (b3PS) ones. The branch lengths of both 6PS and 3PS tiles are two-helical-turn long and the branch lengths of both e3PS and b3PS tiles are four-helical-turn long. The details of the molecular design are shown in Figure S1. The three different 3PS tiles contain different nucleotides (thus, different adsorption strength) and different flexibility.

DNA self-assembly was conducted in two distinct steps according to a reported method:<sup>14,15</sup> (i) assembly of the individual DNA motifs (3PS and 6PS) separately in solution and then (ii) surface-assisted self-assembly of DNA arrays after mixing the two, preassembled DNA tiles. The formation of the individual 3PS series and 6PS was confirmed by native polyacrylamide gel electrophoresis, PAGE, and the assembled DNA networks were directly imaged by AFM in fluid.

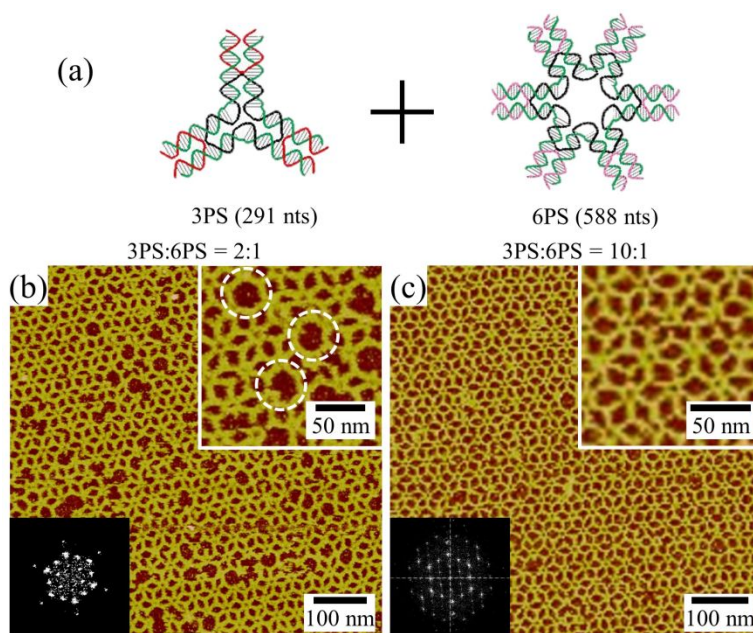


**Figure 2.** Binary assembly of 3PS and 6PS. (a) Structural schemes of the component DNA tiles. AFM images of the DNA networks assembled from 3PS:6PS at molar ratio of (b) 2:1 and (c) 10:1 in bulk solution. White circles in (b) highlight the absence of 3PS tiles.

For the proposed binary assembly of rhombille tiling of 3PS and 6PS, it was most straightforward for the two tiles to have the same branch length as 3PS and 6PS. Each individual tile readily formed as shown by native PAGE (Figures S2 and S3). Separately, each motif can hardly assemble into large arrays by associating with each other due to sticky-end mismatch (Figures S4 and S5). Note that 3PS tiles are too small to adsorb on the surface as individuals, which in turn facilitates the formation of small arrays presumably using their inter-motif base stacking. However, such interactions were weak due to sticky-end mismatch and could easily destabilize the inter-motif cohesion (Figure S4c). When 3PS and 6PS were mixed at the molar ratio of 2:1, rhombille tiling formed (Figures 2b). Surprisingly, 3PS tiles were obviously not enough and were missing in the arrays (deficiency highlighted in circles). Then we realized that 6PS (588 nts) had  $\sim$  twice the size as 3PS (291 nts), leading to a stronger surface adsorption of 6PS than that of 3PS. The differential adsorption caused that the molar ratio of effective surface concentrations of 3PS to 6PS was significantly lower than that of the bulk solution concentration. One possible method to eliminate the 3PS deficiency was to increase the ratio of 3PS to 6PS (3PS:6PS) in bulk solution. When the overall 3PS:6PS ratio increased to 4:1, there was no observable improvement (Figure S6). At 3PS:6PS = 7:1, the 3PS deficiency still existed (Figure S7). Meanwhile, 6PS deficiency started to appear (highlighted by squares). When 3PS:6PS ratio

increased 10:1, both 3PS and 6PS tiles were significantly missed (Figure S8). Yet, in certain small areas, defect-free binary lattices could be observed (Figure 2c). This experiment indicated that tuning the molar ratio of the two tiles in bulk solution was not an effective approach, presumably because there was no clear quantitative description between the effective surface concentration and the bulk solution concentration of the DNA tiles, particularly when two different tiles were involved.

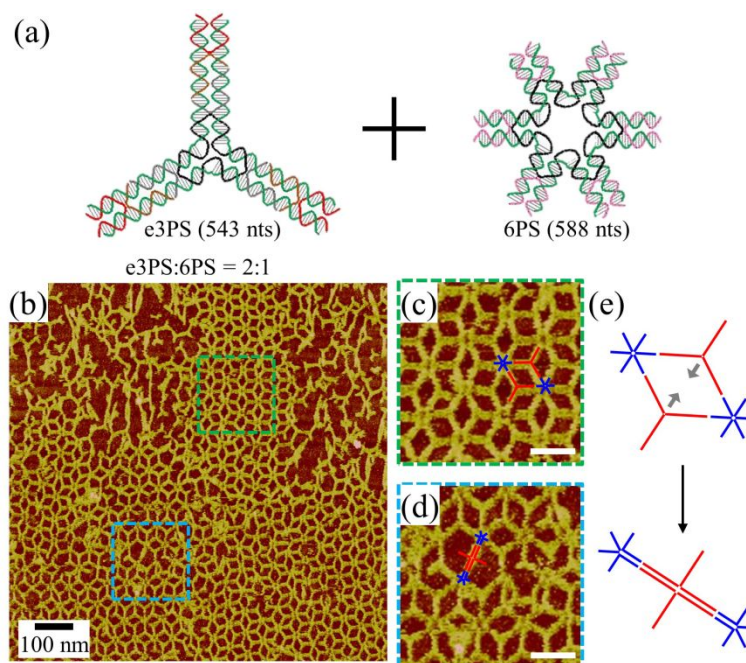


**Figure 3.** Binary assembly of e3PS and 6PS at molar ratio of 2:1 in bulk solution. (a) Structural schemes of e3PS and 6PS. (b) AFM image of the DNA networks. Close-up views of (c) regular motifs and (d) deformed motifs in the corresponding colored boxes from (b). Scale bar: 50 nm. (e) Deformation of (d) from regular rhombus shapes. The grey-colored arrows indicate the deforming orientations.

The problem of the binary assembly of 3PS and 6PS was the differential surface adsorption of the two tiles caused by the large difference of the tile molecular weight. Another approach was to make the two component tiles (3PS and 6PS) have similar sizes. Thus, we elongated the branches of 3PS to  $\sim 4$ -turn long (e3PS), which (543 nts) had a similar size to 6PS (588 nts), as shown in Figure S1a and c. Similar sizes of the two tiles ensure nearly equal strength of surface adsorption. No array was assembled from e3PS tile alone due to the sticky-end mismatch (Figure S9). When e3PS and 6PS were mixed at molar ratio of 2:1 in bulk solution, binary lattices formed with no obvious e3PS or 6PS deficiency (Figures 3 and S10). Even when the overall e3PS:6PS ratio decreased to 1:1, no obvious e3PS deficiency was observed (Figure S11), which indicated that the influence of tile adsorption strength overwhelmed that of tile molar ratio on the lattice formation. Because of the elongated branches in e3PS, the rhombic holes of the rhombille tiling became larger (Figure 3c). However, the large size of the e3PS brought in another problem: this tile's flexibility also increased, which led to a large amount of structural defects and irregularities in the arrays. One particular type of structural deformation was that two

branches of e3PS stacked onto each other at the center of the tile to form pseudo-continuous DNA helixes (Figure 3d). Figure 3e illustrates that two adjacent branches of 6PS rearrange parallel to each other thus eliminate a rhombic cavity.

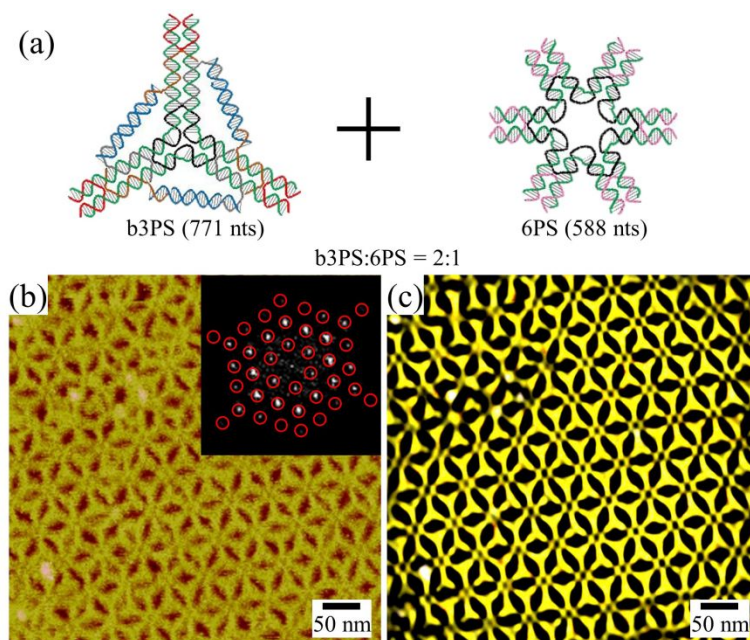


**Figure 4.** Binary assembly of b3PS and 6PS at molar ratio of 2:1 in bulk solution. (a) Structural schemes of b3PS and 6PS. (b) AFM image of the DNA array. (c) Inverse fast Fourier transform (FFT) image of (b) from diffraction spots highlighted in the red circles.

To overcome the flexibility issue, we introduced bridges between adjacent branches in e3PS tiles as inter-branch bridges that could enhance the rigidity of DNA point-star motifs.<sup>16,17</sup> In the new bridged tile (b3PS), the bridges are rigid, 36-bp-long DNA duplexes, which fixed the inter-branch angle to approximately  $60^\circ$  (Figure S1d). The same as other tiles, b3PS could not assemble into large arrays due to sticky-end mismatch (Figure S12). When b3PS and 6PS are mixed at the molar ratio of 2:1 in bulk solution, large, defect-free binary arrays formed (Figures 4 and S13). Rigidity of the b3PS tile ensured the integrity of binary arrays. Note that though the b3PS motif (771 nt) is approximately 20% larger than the 6PS motif (588 nt), such difference is too small to affect the formation of binary arrays.

In order to develop a better understanding of the assembled DNA rhombille tiling, we conducted the fast Fourier transform (FFT) of a defect-free, single 2D crystal assembled from the b3PS and 6PS tiles (Figure S14a). A clear 6-fold symmetry existed in the FFT pattern (Figure S14b). Yet the two different types of vertices (3PS and 6PS) express their own symmetries independently. The inverse FFT analysis of the most inner ring of diffraction spots (highlighted by red circles in Figure S14b) shows the reconstructed lattice of 6PS motifs (Figure S14c), while that of the second most inner ring (highlighted by blue circles in Figure S14b) renders the lattice of b3PS motifs (Figure S14d). The inverse FFT images also agree with the AFM image at corresponding positions highlighted by green circles and pink squares (Figure S14a, c, d).

In the binary lattices assembled from b3PS, interesting bridge exchanges were observed (Figure S15). In most cases, b3PS motifs existed intact as designed (Figure S15b). Some b3PS motifs exchange their bridges with adjacent b3PS motifs to form dimeric b3PS motifs (Figure S15c). Such b3PS dimer also existed in solution as shown in native PAGE (Figure S3). This bridge exchange would theoretically shift the inter-branch angle from 60° to 49° (Figure S16), but this angle variation was sufficiently small and did not significantly impact on the array formation.

In summary, we have developed a rational strategy to overcome the differential adsorption problem of different DNA motifs to assembled DNA binary arrays on solid surface. The keys of this study are: (1) Balance the surface adsorption of different DNA motifs; (2) Enhance the rigidity of DNA lattices. We envision that this strategy will facilitate assembly of complex DNA nanostructures that require multiple different tiles.<sup>18,19</sup>

**Acknowledgement.** This work was supported by the National Science Foundation (CCF-2107393 and CCFMI-2025187).

## References

1. E. Winfree, F. Liu, L. A. Wenzler and N. C. Seeman. *Nature*, 1998, **394**, 539–544.
2. H. Yan, S. H. Park, G. Finkelstein, J. H. Reif and T. H. LaBean. *Science*, 2003, **301**, 1882–1884.
3. L. Yu, J. Cheng, D. Wang, V. Pan, S. Chang, J. Song and Y. Ke. *J. Am. Chem. Soc.*, 2022, **144**, 9747–9752.
4. S. Li, Y. Wang, W. Ge, W. Zhang, B. Lu, F. Feng, C. Ni and S.-J. Xiao. *Chem. Eur. J.*, 2023, **29**, e202202863.
5. C. Lin, E. Katilius, Y. Liu, J. Zhang and H. Yan. *Angew. Chem. Int. Ed.*, 2006, **45**, 5296–5301.
6. W. Wang, C. Chen, S. Vecchioni, T. Zhang, C. Wu, Y. P. Ohayon, R. Sha, N. C. Seeman and B. Wei. *Angew. Chem. Int. Ed.*, 2021, **60**, 25781–25786.
7. S. H. Park, P. Yin, Y. Liu, J. H. Reif, T. H. LaBean and H. Yan. *Nano Lett.*, 2005, **5**, 729–733.
8. Y. Li, L. Song, B. Wang, J. He, Y. Li, Z. Deng and C. Mao. *Angew. Chem. Int. Ed.*, 2018, **57**, 6892–6895.
9. W. Liu, H. Zhong, R. Wang and N. C. Seeman. *Angew. Chem. Int. Ed.*, 2011, **50**, 264–267.
10. P. Wang, S. Gaitanaros, S. Lee, M. Bathe, W. M. Shih and Y. Ke. *J. Am. Chem. Soc.*, 2016, **50**, 264–267.
11. X. Sun, S. Hyeon Ko, C. Zhang, A. E. Ribbe and C. Mao. *J. Am. Chem. Soc.*, 2009, **131**, 13248–13249.
12. S. Hamada and S. Murata. *Angew. Chem. Int. Ed.*, 2009, **48**, 6820–6823.
13. L. Liu, Y. Li, Y. Wang, J. Zheng and C. Mao. *ChemBioChem*, 2017, **18**, 2404–2407.
14. N. Avakyan, J. W. Conway and H. F. Sleiman. *J. Am. Chem. Soc.*, 2017, **139**, 12027–12034.
15. G. Tikhomirov, P. Petersen and L. Qian. *Nature*, 2017, **552**, 67–71.
16. L. Liu, Z. Li, Y. Li and C. Mao. *J. Am. Chem. Soc.*, 2019, **141**, 4248–4251.

17. L. Liu, M. Zheng, Z. Li, Q. Li and C. Mao. *ACS Appl. Mater. Interfaces.*, 2019, **11**, 13853–13858.
18. F. Zhang, Y. Liu and H. Yan. *J. Am. Chem. Soc.*, 2013, **135**, 7458–7461.
19. D. Woods, D. Doty, C. Myhrvold, J. Hui, F. Zhou, P. Yin and E. Winfree. *Nature*, 2019, **567**, 366–372.